Sahel decadal rainfall variability and the role of model horizontal resolution

Vellinga, M., Roberts, M., Vidale, P. L. ORCID: https://orcid.org/0000-0002-1800-8460, Mizielinski, M. S., Demory, M.-E., Schiemann, R. ORCID: https://orcid.org/0000-0003-3095-9856, Strachan, J. and Bain, C. (2016) Sahel decadal rainfall variability and the role of model horizontal resolution. Geophysical Research Letters, 43 (1). pp. 326-333. ISSN 0094-8276 doi: https://doi.org/10.1002/2015GL066690 Available at https://centaur.reading.ac.uk/51837/

AGU PUBLICATIONS

Geophysical Research Letters

RESEARCH LETTER
10.1002/2015GL066690

Key Points:
- Most global climate models underestimate twentieth century Sahel decadal rainfall changes
- Increased atmosphere resolution raises amplitude of model variability to observed levels
- Key circulation-rainfall interactions better represented with higher resolution

Supporting Information:
- Supporting Information S1
- Figure S1
- Figure S2
- Figure S3
- Figure S4

Correspondence to:
M. Vellinga,
michael.vellinga@metoffice.gov.uk

Citation:
Vellinga, M., M. Roberts, P. L. Vidale, M. S. Mizielinski, M.-E. Demory, R. Schiemann, J. Strachan, and C. Bain (2015), Sahel decadal rainfall variability and the role of model horizontal resolution, *Geophys. Res. Lett.*, *42*, doi:10.1002/2015GL066690.

Received 21 OCT 2015
Accepted 6 DEC 2015

Sahel decadal rainfall variability and the role of model horizontal resolution

Michael Vellinga[1], Malcolm Roberts[1], Pier Luigi Vidale[2], Matthew S. Mizielinski[1], Marie-Estelle Demory[2], Reinhard Schiemann[2], Jane Strachan[1], and Caroline Bain[1]

[1]Met Office Hadley Centre, Exeter, UK, [2]NCAS Climate, University of Reading, Reading, UK

Abstract Substantial low-frequency rainfall fluctuations occurred in the Sahel throughout the twentieth century, causing devastating drought. Modeling these low-frequency rainfall fluctuations has remained problematic for climate models for many years. Here we show using a combination of state-of-the-art rainfall observations and high-resolution global climate models that changes in organized heavy rainfall events carry most of the rainfall variability in the Sahel at multiannual to decadal time scales. Ability to produce intense, organized convection allows climate models to correctly simulate the magnitude of late-twentieth century rainfall change, underlining the importance of model resolution. Increasing model resolution allows a better coupling between large-scale circulation changes and regional rainfall processes over the Sahel. These results provide a strong basis for developing more reliable and skilful long-term predictions of rainfall (seasons to years) which could benefit many sectors in the region by allowing early adaptation to impending extremes.

1. Introduction

The Sahel is prone to substantial fluctuations in monsoon (July–September mean) rainfall, at interannual to decadal timescales. Climate models have successfully demonstrated the importance of sea surface temperature (SST) in driving Sahel rainfall variability at these timescales [*Folland et al.*, 1986; *Giannini et al.*, 2003; *Mohino et al.*, 2011]. However, a long-standing problem has been that most global climate models underestimate the magnitude of decadal variability in the twentieth century simulations [*Biasutti*, 2013; *Roehrig et al.*, 2013]. This weak magnitude of decadal rainfall variability in models is not well understood and has received little attention, in spite of obvious implications for multiannual predictions or detection and attribution of observed Sahel rainfall change. Weak decadal variability in coupled models may be attributed to models' inability to generate realistic decadal SST variability [*Martin et al.*, 2014]. However, in global atmosphere-only models in which SST is prescribed the problem also widely occurs [*Scaife et al.*, 2008] which points to an unrealistically weak teleconnection between SST change and Sahel rainfall.

Most of the rainfall during the monsoon season comes from organized convection, such as squall lines and large mesoscale convective systems (MCS) [*Mathon et al.*, 2002]. Resolution in most Climate Model Intercomparison Project Phase 5 (CMIP5) [*Taylor et al.*, 2012] atmosphere models is 150 km or coarser, barely enough to resolve the largest convective systems during their mature phase, let alone their development phase. It is unclear whether this matters for simulating Sahel rainfall variability over seasons to years. When coarse-resolution climate models are used to study Sahel rainfall, this therefore makes the implicit assumption that any convection, organized or not, is sufficient to interact with the large-scale circulation to contribute to moisture convergence over this semiarid region. Previous work has shown improvements in the time-mean, global-mean moisture convergence over land with increased horizontal resolution [*Demory et al.*, 2014]. The sensitivity of regional-scale, Sahel decadal rainfall change to resolution has not been studied previously but the importance of multiscale interactions between convection and regional circulation for rainfall extremes [*Cretat et al.*, 2014], African easterly waves (AEWs) [*Berry and Thorncroft*, 2012], or the monsoon's moisture budget [*Birch et al.*, 2014] in regional models underlines the importance of high resolution. Climate predictions and projections require global models to represent local and remote drivers of rainfall change and any interaction between the two. This is our main motivation for investigating the role of increasing resolution in a global model setup.

Here we investigate the role of atmosphere horizontal resolution for simulating Sahel decadal rainfall variability. Specifically, we ask if the amplitude of decadal rainfall variability can be improved by increasing horizontal resolution. We focus on the atmospheric response to forcing by SST and do not address prediction of decadal SST anomalies.

2. Methods

We examine the 25 year period 1984–2008 when Sahel rainfall recovered from the preceding severe drought to near-normal conditions. We use 10–20°N, 15°W–30°E to define the Sahel region in this study. Observations from five data sets (GPCP_vn2.2 [*Adler et al.*, 2003], GPCC [*Schneider et al.*, 2014], TAMSAT [*Tarnavsky et al.*, 2014], CRUTS_vn3.22 [*Harris et al.*, 2014], and GHCND [*Mitchell*, 2013]) put the decadal rainfall trend between 1984 and 2008 to around 7–11 mm/month/decade for July–September means in the Sahel. We use three global atmosphere model configurations [*Mizielinski et al.*, 2014] of the Met UM atmosphere model (HG) [*Walters et al.*, 2011] that are identical, except for their horizontal resolution. Therefore, we can unambiguously attribute differences in rainfall change between these configurations to resolution, not confounded by differences in model physics. This is a strong advantage over multimodel ensembles such as CMIP5 [*Taylor et al.*, 2012], where the causes of intermodel differences can be numerous and often difficult to isolate. The models are forced by high-resolution, daily SST from OSTIA [*Donlon et al.*, 2012] and further follow the AMIP-II protocol of CMIP5 (using prescribed, historical sea ice, greenhouse gas, and aerosol concentrations for the period 1985–2008).

By using historical SST and other forcings, we can make a direct comparison between observed and simulated rainfall. This is in contrast with experiments with coupled models, where SST can evolve freely and need not follow the evolution of real-world twentieth century SST. Prescribing SST also avoids the problem of introducing SST biases that affect coupled models and contribute to errors in precipitation. HG was run at three resolutions, referred to by their resolution at midlatitudes: 130 km (HG130), 60 km (HG60), and 25 km (HG25). We ran multiple model realizations at each resolution and use ensemble means to better estimate the model response to the forcing. There are four, three, and five ensemble members for HG130, HG60, and HG25.

3. Results

Ensemble-mean decadal trends of Sahel rainfall in HG are shown in Figure 1a. There is a strong dependence on resolution: HG130 underestimates the trend whereas the HG60 and HG25 show stronger trends that are within the observed range. The atmospheric moisture budget (Figure S1 in the supporting information) shows that increasing resolution has two effects: first, there is stronger decadal increase in moisture fluxes across the region's boundaries. Second, at 130 km resolution 62% of the moisture transported into the region escapes again without precipitating, whereas at 25 km this reduces to 37%. In other words, the high-resolution model is almost twice as efficient at generating precipitation from the extra available moisture supplied by the large-scale circulation compared to the low-resolution model. The efficient moisture convergence over the Sahel at high resolution is caused by a much stronger coupling between convective rainfall and circulation changes than is seen at low resolution. We investigate this by quantifying subdaily rainfall events (section 3.1) and their relation to the large-scale circulation (section 3.2).

3.1. Subdaily Rainfall

The combination of satellite-born radar, microwave, and infrared observations into TRMM_3B42_vn7 [*Huffman et al.*, 2007] (Tropical Rainfall Measuring Mission (TRMM)) precipitation yields high spatiotemporal resolution: $\frac{1}{4}°$, 3-hourly for 1998–2013. Averaging TRMM over the north-south extent of the Sahel reveals strong spatiotemporal coherency of rainfall systems (Figure 2c). Rainfall is predominantly organized in large coherent structures that travel mostly westward, with lifetimes from hours to days. Rainfall in HG130 is organized very differently: it occurs synchronously across the region, with 3-hourly intensities generally weaker than observed (Figure 2a). At 25 km resolution, weak stationary features still occur, but now westward propagating, intense convective systems are also present (Figure 2b). Distributions of 3-hourly rainfall intensity show that compared to TRMM the HG models underestimate the frequency of intense rainfall events and overestimate the frequency of weak events. The crossover point lies at around 0.5 mm/h (Figure 3). The probability of an individual 3-hourly event >0.5 mm/h (shown by the numbers in legend) increases with model resolution and gets closer to that of TRMM. This sensitivity to resolution also occurs if 3-hourly rainfall is first aggregated onto the coarsest HG130 grid (numbers in brackets). None of the HG130,HG60, and HG25 configurations replicates the heavy right tail in TRMM, but these events are rare.

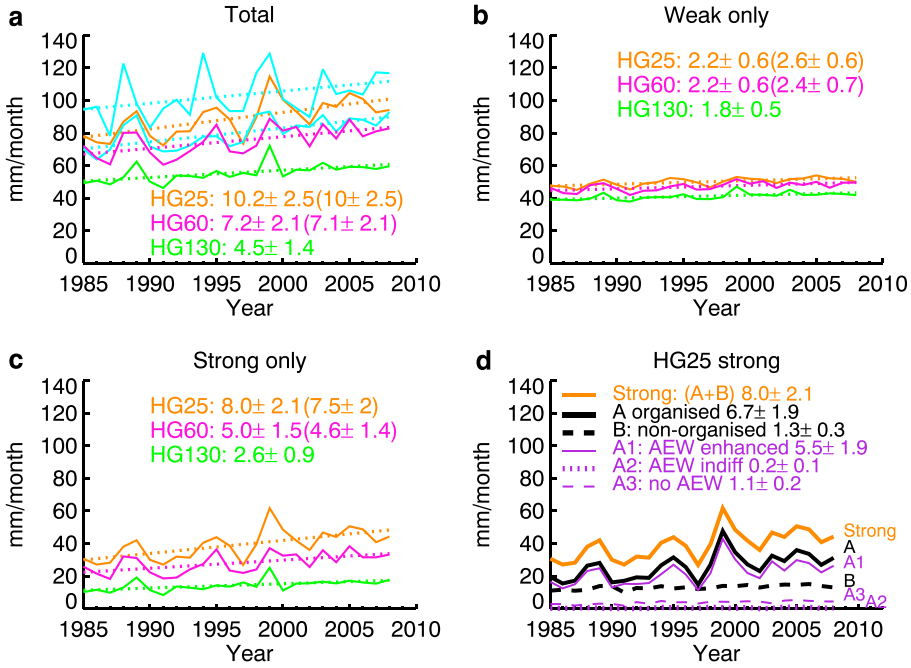

Figure 1. July–September Sahel mean rainfall time series. (a) Total rainfall in the 130 km (green), 60 km (magenta), and 25 km (amber) HG configurations and observations (upper cyan curve CRUTS, lower cyan curve TAMSAT). Corresponding linear trends (mm/month/decade) and standard error are shown by the numbers (numbers in brackets are equivalent values when precipitation is first regridded onto the HG130 grid). (b) As Figure 1a but only counting contributions from weak 3-hourly events (<0.5 mm/h). (c) As Figure 1a but only counting contributions from strong 3-hourly events (>0.5 mm/h). (d) Decomposition of rainfall from strong 3-hourly events in HG25 (amber curve Figure 1c), shown again in Figure 1d by the heavy amber curve. It is split into rainfall from organized events (black solid, line A) and nonorganized events (black dashed, line B). Organized rainfall (A) is decomposed into organized events enhanced by African easterly waves (purple solid, line A1), organized events that are insensitive to passing AEWs (purple dotted, line A2), and organized events that occur without any AEW activity nearby (purple dashed, line A3). Thus, curve A is sum of purple curves A1-3 and the amber curve is sum of black curves A and B. Method described in Text S1. Data are ensemble means calculated from decompositions of individual ensemble members.

The importance of subdaily rainfall events becomes clear when we accumulate them over the multidecadal period. Using the crossover point of 0.5 mm/h in Figure 3 as a threshold, we calculate decadal rainfall time series due to weak (<0.5 mm/h) and strong (>0.5 mm/h) 3-hourly events (Figures 1b and 1c) and determine their decadal trends. Weak events contribute most to the average rainfall in the Sahel, particularly at low resolution, but their contribution does not change much over time (about 2 mm/month/decade, Figure 1b). Most of the total trend comes from the trend in strong events: at 25 km resolution, 8 mm/month/decade or 80% of the overall trend (Figures 1b and 1c). Again, these numbers change little (2–8%) if precipitation is first aggregated on the coarsest (HG130) grid, (Figures 1a–1c trends in brackets) showing this resolution dependence is not a by-product from sampling rainfall on a higher-resolution grid, but an inherent property of the high-resolution configuration. Further decomposition of strong events shows that at 25 km most (> 80%) of the trend in strong rainfall occurs as organized convection: rainfall events that are coherent in space and time (heavy black curve in Figure 1d and method described in the supporting information Text S1). A further decomposition of heavy rainfall events and their relation with dynamical features of the circulation are presented next.

3.2. Circulation Changes

The historical SST by which the atmosphere models are forced drive an anomalous Walker circulation between the Eastern Pacific and Atlantic (supporting information Figure S2). Circulation changes over Africa below 850 hPa are westerly from the Atlantic, easterly above 700 hPa, including an intensification of the African Easterly Jet (AEJ). Stronger low-level westerlies bring more moisture to the region, supporting increased rainfall [*Pu and Cook*, 2012]. In contrast, a strengthening of the AEJ is expected to reduce rainfall by strengthening moisture divergence [*Cook*, 1999; *Grist and Nicholson*, 2001]. Finally, synoptic African Easterly Wave (AEW) disturbances on the AEJ [*Burpee*, 1972] are also important because they provide low-level convergence that can

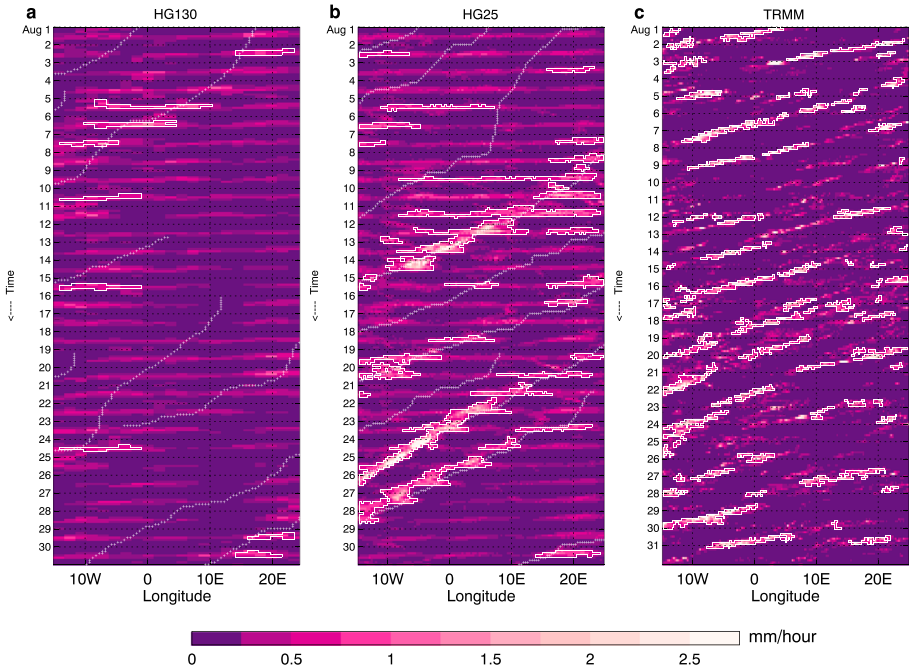

Figure 2. Examples of typical rainfall sequences. Meridionally averaged (10–20°N) 3-hourly rainfall shown as a function of longitude (horizontal) and time (vertical, positive down) for single members of (a) HG130, (b) HG25, and (c) TRMM. Organized rainfall objects are outlined by white contours; African easterly wave tracks in the models are shown by white crosses.

support convective rainfall [*Duvel*, 1990; *Fink and Reiner*, 2003]. Conversely, convection itself is instrumental for the wave dynamics by modifying the potential vorticity (PV) field near the wave [*Berry and Thorncroft*, 2005]. This is important for wave initiation [e.g., *Hsieh and Cook*, 2007; *Thorncroft et al.*, 2008] and subsequent maintenance of the wave [e.g., *Hsieh and Cook*, 2007; *Berry and Thorncroft*, 2012].

We determine AEW activity in HG3 using the automated tracking described by *Bain et al.* [2013]. We observe an increase in the number of strong AEWs in HG25 of about 12% decade (Figure 4a). The lower resolution models have no significant trend in the number of AEWs (Figure 4a). This sensitivity of AEWs to resolution is important because much of the decadal trend of strong rainfall events (Figure 1d, amber line) in HG25 is associated with organized rainfall that is strengthened or initiated by AEW disturbances (about 70%, solid purple line A1 in

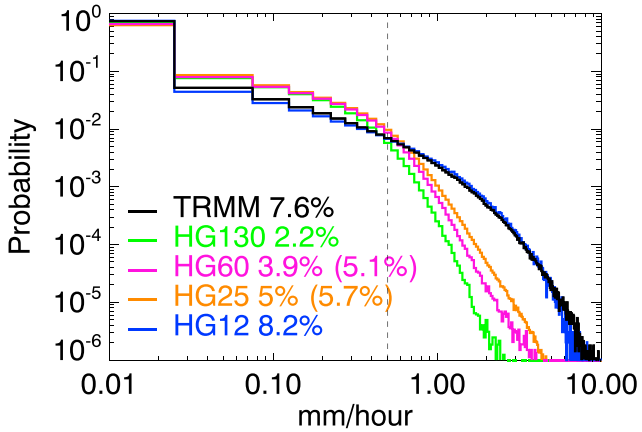

Figure 3. Distributions of 3-hourly meridional mean Sahel rainfall in July–September. TRMM is for years 1998–2013 and is shown in black. The HG130, HG60, and HG25 models use all ensemble members for years 1985–2011. HG12 uses one realization for years 2008–2011. Numbers in the legend are the probability for an event >0.5 mm/h (dashed line) in each of the distributions; number in brackets is the probability when rainfall is first aggregated onto the HG130 grid.

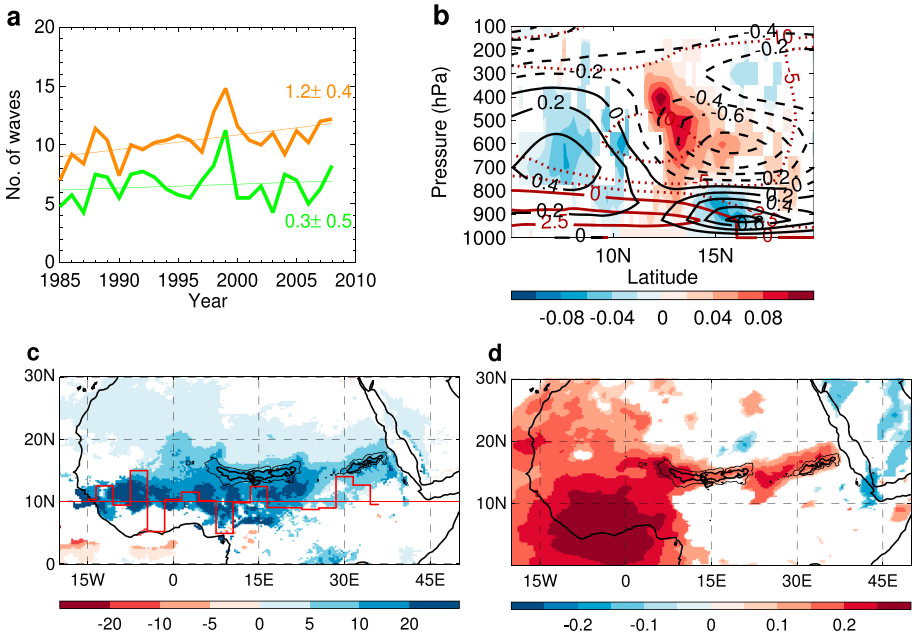

Figure 4. Decadal changes in AEJ and AEWs in HG25, all calculated for July–September (JAS) ensemble means between 1985 and 2008. Data not significant at the 5% level is masked. (a) Total number of strong AEWs occurring over land (15°W–30°E). Amber is HG25, and green HG130. AEWs were tracked in individual members using data regridded onto a common grid of 0.5°. Waves are designated as strong if, over their lifetime, their median strength exceeds the median strength of the full AEW population. Numbers are decadal trend and standard error. (b) Colors: linear trend of Φ, the fraction of the domain with a negative potential vorticity gradient between 15°W and 30°E (see supporting information Text S1). We evaluate Φ in JAS mean flow each year in individual members then calculate the decadal trend of the ensemble mean. Black contours show the trend in zonal mean flow (in m/s/decade, negative dashed). Brown contours show climatological mean zonal mean wind (m/s, negative contours dotted). (c) Trend in mean monthly rainfall (colors, mm/month/decade) and mean maximum daily rainfall (contours of increasing thickness at 12.5, 15, and 17.5 mm/d/decade). Red histograms centered around 10°N show the trend in the numbers of AEWs formed relative to the long-term mean at each longitude. A deflection of ±1° corresponds to ±5/%decade. (d) Trend in 3–5 day band-pass-filtered variance of 700 hPa meridional velocity in JAS, expressed as a fraction of the long-term ensemble mean variance.

Figure 1d). In HG60 and HG130 this reduces to 64% and 46%, respectively. Interaction between dynamics and organized rainfall in HG is evidently more efficient at high resolution. Because of the strong interaction between AEWs and convection causality of their decadal change is difficult to establish and beyond the scope of this paper. Nevertheless, the clear resolution dependence of rainfall change in HG and the use of identical physics across resolution point to essential differences in how this interaction changes over time between HG25 and HG130.

Intense convection has been linked to AEW initiation by reversing PV gradients [e.g., *Hsieh and Cook*, 2007]. In HG25 there are two areas in the center and east of the region where the largest decadal increase in daily maximum rainfall (a proxy for the most intense convection) is concentrated (Figure 4c, contours). Particularly in the easternmost area this coincides with an increase in the number of AEWs formed (Figure 4c, red histogram). The largest increase in seasonal mean rainfall is farther to the west and south without clear relation to changes in AEW formation, perhaps reflecting a different stage of AEW-rainfall interaction compared to maximum daily rainfall. The magnitude of 3–5 day AEW variability increases across the Sahel with local maxima directly downstream of both regions of greatest daily maximum rainfall increase (Figure 4d). In HG130 the decadal increase in daily maximum rainfall, its link to AEW formation, and overall AEW activity increase are weaker than HG25 (or fully absent) even when HG25 is aggregated onto the HG130 grid (Figure S3). Finally, the large-scale tropical circulation changes (Figures S2b and S2c) result in increased shear on the AEJ (Figure 4b) which supports stronger barotropic and baroclinic energy conversions for AEWs. Again, these changes are strongest at high resolution (HG130 shown in Figure S3f). Our overall conclusion is that key local-scale and large-scale interactions between rainfall and dynamics are much more effective at higher resolution. These interactions

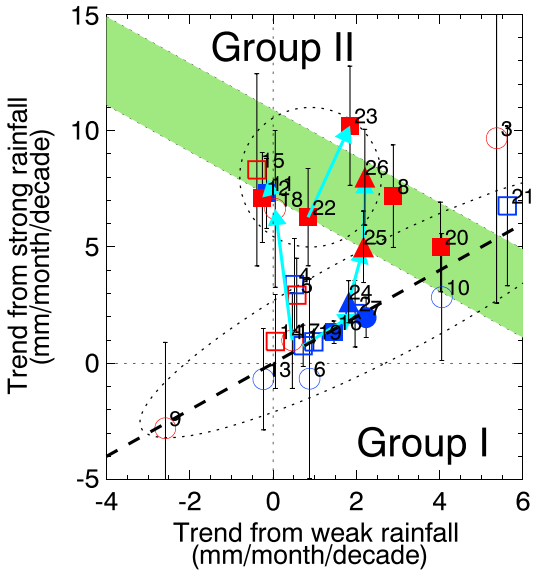

Figure 5. Trend from 1984 to 2008 (July–September) carried by weak (<0.5 mm/h, abscissa) and strong (>0.5 mm/h, ordinate, grey bars show standard error) 3-hourly rainfall for CMIP5 AMIP experiments (circles for models with one member and squares for ensemble means) and HG (triangles). Key to model numbers is in the supporting information Table S1. Solid symbols indicate models where the overall trend (sum of weak + strong events) is statistically significant at the 5% level. Models where organized rainfall carries more (less) than 50% of overall trend are shown in red (blue). Cyan arrows connect model configurations of increased horizontal resolution. Dashed line is 1-1 diagonal. Green area spans the region consistent with the observed range of the overall trend.

underpin the more realistic decadal rainfall variability in HG25.

4. CMIP5 Results

We use the results from HG as a framework to chart the behavior of CMIP5 AMIP (i.e., atmosphere-only) simulations. We apply the same decomposition into weak/strong 3-hourly rainfall events to AMIP simulations with 23 CMIP5 models for 1984–2008 (Figure 5, model details are provided in the supporting information Table S1). First, we note that only 8/23 CMIP5 models have a decadal overall trend that is significantly different from zero (at the 5% level, solid symbols) and only 4/23 lie within the observed range (green shading). This reiterates the difficulty for CMIP5 AMIP models to represent the twentieth century decadal trend, as noticed previously by *Roehrig et al.* [2013] but shown here for absolute (i.e., nonnormalized) trends using ensemble means where available (squares). Second, CMIP5 models broadly cluster into two groups: group I where weak and strong 3-hourly rainfall events are of comparable importance for the decadal overall trend and group II where most of the overall trend comes from strong events and weak events only have a small decadal trend (<2.5 mm/month/decade). Models that are closest to the observed trends (green region) are mostly from group II, i.e., with dominant contributions from strong 3-hourly events. Furthermore, in most group II models (6/7) organized convection dominates the net trend (red symbols). Finally, four CMIP5 models use multiple configurations of low/high resolution, connected by cyan arrows in Figure 5. Increasing resolution generally increases the overall rainfall trend and can even move models from group I to group II. A caveat on this is that unlike in the HG ensemble, in CMIP5 different resolutions sometimes do use different model parameter values [e.g., *Hourdin et al.*, 2012] confounding the effect of increased resolution.

The CMIP5 results thus span the behavior of the three HG configurations (triangles in Figure 5): (i) in models with a realistic decadal overall precipitation trend, strong 3-hourly rainfall events generally carry most of this trend; (ii) increasing resolution raises the importance of strong rainfall events and results in a stronger overall decadal trend. Model physics are clearly important, too, as is evident from the range of model resolutions of Group II models. We interpret the multimodel results as showing that higher resolution gives model physics the scope to better represent the processes driving Sahel rainfall change. The quantitative effect of increasing resolution on Sahel precipitation in each model depends on its physics (e.g., coupling between AEWs and precipitation) [*Skinner and Diffenbaugh*, 2013].

5. Discussion

We have identified a crucial interaction across temporal and spatial scales that models need to represent to realistically simulate the cycle of multiannual wet and dry phases in the Sahel. Strong, convective rainfall events (hours, localized), through their effect on organized convection and interaction with the circulation (days, hundreds to thousands of kilometers) communicate the effects of low-frequency, SST-driven circulation changes (years, global scale) to the Sahel. This multiscale interaction explains the long-standing difficulty of global climate models to represent decadal Sahel rainfall variability realistically: sufficient resolution is essential to adequately represent the interaction between large-scale and small-scale dynamics to allow large-scale

SST forcing to exert its influence. These requirements on model physics and model resolution are computationally extremely demanding on a global domain but have increasingly started to come within the reach of the modeling community's capabilities [*Kinter and authors*, 2013; *Mizielinski et al.*, 2014].

We find that interaction between circulation and organized rainfall in HG is more efficient at high resolution. Our results suggest that we should exercise caution when using coarse-resolution models to study Sahel rainfall as they may underrepresent the interaction between convection and dynamics that contributes to regional moisture convergence. This may, for example, express itself as an apparent insensitivity of Sahel rainfall to decadal SST change.

An improved response by the atmosphere to the changes in SST, so important for Sahel rainfall, reduces an important source of uncertainty in predictions for the region. Predicting SST change at longer lead times is clearly uncertain, but an improved response of rainfall to SST is a necessary step toward an improved physical basis for predictions of Sahel rainfall of seasons to years. The prospect of better predictions is long overdue, given the strong requirements for reliable climate information for this region that can inform adaptation against future cycles of droughts and wet phases.

We have shown that increasing resolution from HG130 to HG25 significantly improves decadal rainfall change. Yet even HG25 misses some rainfall processes over the Sahel, e.g., it underrepresents extreme 3-hourly rainfall events compared to TRMM (Figure 3) and misrepresents the phase of the mean diurnal cycle, as do all group II CMIP5 models (Figure S4). While obviously undesirable this suggests that the phasing of the diurnal cycle is in itself not a crucial factor for representing decadal variability of seasonal mean rainfall. This need not be true for other climate phenomena such as extreme rainfall. We found that these problems do not occur in a global 12 km convection-permitting configuration of HG (model setup described in the supporting information Text S2 and *Birch et al.* [2015]). It matches TRMM extremely well (Figure 3, blue curve) over the Sahel, and its improved representation of subdaily rainfall results in a much improved diurnal cycle of Sahel rainfall (Figure S4) and generally in the tropics [*Birch et al.*, 2015]. This suggests that a step change in representing rainfall in the Sahel may be possible in convection permitting global model configurations, consistent with other pioneering studies of tropical phenomena [e.g., *Taniguchi et al.*, 2010]. We will continue to explore the challenges and benefits of improving representation of rainfall processes for modeling climate variability over Africa and elsewhere in future work.

Acknowledgments

M.V. and C.B. were supported by the joint UK DFID/ Met Office Hadley Centre Climate Science Research Partnership (CSRP), funded by the UK Department for International Development (DFID) for the benefit of developing countries. The views expressed are not necessarily those of DFID. M.R. and M.S.M. were supported by the Joint UK DECC/DEFRA Met Office Hadley Centre Climate Programme (GA01101). P.L.V. and M.E.D. acknowledge NCAS Climate contract R8/H12/83/001 for the High Resolution Climate Modelling programme. R.S. acknowledges NERC-Met Office JWCRP HRCM funding. P.L.V. (UPSCALE PI) acknowledges the Willis Chair in Climate System Science and Climate Hazards that supports his research. We thank the team of model developers and infrastructure experts required to conduct the large-scale HG simulation campaign and acknowledge use of the MONSooN system, a collaborative facility supplied under the JWCRP; the PRACE infrastructure; the Stuttgart HLRS supercomputing center, and the STFC CEDA service for data storage and analysis using the JASMIN platform. We thank Jamie Kettleborough, Emma Hibling, Peter Good, and Ian Edmond for facilitating the CMIP5 data retrieval. We acknowledge the World Climate Research Programme's Working Group on Coupled Modelling, which is responsible for CMIP, and we thank the climate modeling groups (listed in the supporting information Table S1) for producing and making available their model output and their help with our enquiries. For CMIP the U.S. Department of Energy's Program for Climate Model Diagnosis and Intercomparison provides coordinating support and led development of software infrastructure in partnership with the Global Organization for Earth System Science Portals. Comments by Kerry Cook have helped to improve the manuscript and are gratefully acknowledged. Discussions with José Rodriguez, Richard Graham, Adam Scaife, Gill Martin, Lizzie Good, Rob Chadwick, and Steve Woolnough are gratefully acknowledged. The HG experiments were produced as part of the UPSCALE project. Information about project and data access is available from the project website: http://proj.badc.rl.ac.uk/upscale. CMIP5 data used in this study are available via http://cmip-pcmdi.llnl.gov/cmip5/availability.html.

References

Adler, R. F., et al. (2003), The version 2 Global Precipitation Climatology Project (GPCP) monthly precipitation analysis (1979–present), *J. Hydrometeorol.*, *4*, 1147–1167.

Bain, C. L., K. D. Williams, S. F. Milton, and J. T. Heming (2013), Objective tracking of African easterly waves in Met Office models, *Q. J. R. Meteorol. Soc.*, *140*, 47–57, doi:10.1002/qj.2110.

Berry, G., and C. Thorncroft (2012), African easterly wave dynamics in a mesoscale numerical model: The upscale role of convection, *J. Atmos. Sci.*, *69*, 1267–1283, doi:10.1175/JAS-D-11-099.1.

Berry, G. J., and C. Thorncroft (2005), Case study of an intense African easterly wave, *Mon. Weather Rev.*, *133*, 752–766, doi:10.1175/MWR2884.1.

Biasutti, M. (2013), Forced Sahel rainfall trends in the CMIP5 archive, *J. Geophys. Res.*, *118*, 1613–1623, doi:10.1002/jgrd.50206.

Birch, C., D. Parker, J. Marsham, D. Copsey, and L. Garcia-Carreras (2014), A seamless assessment of the role of convection in the water cycle of the West African Monsoon, *J. Geophys. Res.*, *119*, 2890–2912, doi:10.1002/2013JD020887.

Birch, C., M. Roberts, L. Garcia-Carreras, D. Ackerley, M. Reeder, and A. Lock (2015), Sea breeze dynamics and convective initiation: The influence of convective parameterisation on climate model biases, *J. Clim.*, *28*, 8093–8108, doi:10.1175/JCLI-D-14-00850.1.

Burpee, R. W. (1972), The origin and structure of easterly waves in the lower troposphere of North Africa, *J. Atmos. Sci.*, *29*, 77–90, doi:10.1175/1520-0469(1972)029<0077:TOASOE>2.0.CO;2.

Cook, K. (1999), Generation of the African Easterly Jet and its role in determining West African precipitation, *J. Clim.*, *12*, 1165–1184, doi:10.1175/1520-0442(1999)012<1165:GOTAEJ>2.0.CO;2.

Cretat, J., E. Vizy, and K. Cook (2014), How well are daily intense rainfall events captured by current climate models over Africa?, *Clim. Dyn.*, *42*(9), 2691–2711, doi:10.1007/s00382-013-1796-7.

Demory, M.-E., P. L. Vidale, M. Roberts, P. Berrisford, J. Strachan, R. Schiemann, and M. Mizielinski (2014), The role of horizontal resolution in simulating drivers of the global hydrological cycle, *Clim. Dyn.*, *42*, 2201–2225, doi:10.1007/s00382-013-1924-4.

Donlon, C., M. Martin, J. Stark, J. Roberts-Jones, E. Fiedler, and W. Wimmer (2012), The Operational Sea Surface Temperature and Sea Ice Analysis (OSTIA) system, *Remote Sens. Environ.*, *116*, 140–158, doi:10.1016/j.rse.2010.10.017.

Duvel, J. (1990), Convection over tropical Africa and the Atlantic Ocean during northern summer. Part II: Modulation by easterly waves, *Mon. Weather Rev.*, *118*, 1855–1868, doi:10.1175/1520-0493(1990)118<1855:COTAAT>2.0.CO;2.

Fink, A. H., and A. Reiner (2003), Spatiotemporal variability of the relation between African Easterly Waves and West African squall lines in 1998 and 1999, *J. Geophys. Res.*, *108*, 4332, doi:10.1029/2002JD002816.

Folland, C. K., D. E. Parker, and T. N. Palmer (1986), Sahel rainfall and worldwide sea temperatures, *Nature*, *320*, 602–607.

Giannini, A., R. Saravanan, and P. Chang (2003), Oceanic forcing of Sahel rainfall on interannual to interdecadal time scales, *Science*, *302*, 1027–1030, doi:10.1126/science.1089357.

Grist, J., and S. Nicholson (2001), A study of the dynamic factors influencing the rainfall variability in the West African Sahel, *J. Clim.*, *14*, 1337–1359, doi:10.1175/1520-0442(2001)014<1337:ASOTDF>2.0.CO;2.

Harris, I., P. D. Jones, T. J. Osborn, and D. H. Lister (2014), Updated high-resolution grids of monthly climatic observations—The CRU TS3.10 dataset, *Int. J. Climatol.*, *34*, 623–642, doi:10.1002/joc.3711.

Hourdin, F., et al. (2012), Impact of the LMDZ atmospheric grid configuration on the climate and sensitivity of the IPSL-CM5A coupled model, *Clim. Dyn.*, *40*, 2167–2192, doi:10.1007/s00382-012-1411-3.

Hsieh, J.-S., and K. Cook (2007), A study of the energetics of African easterly waves using a regional climate model, *J. Atmos. Sci.*, *64*, 421–440, doi:10.1175/JAS3851.1.

Huffman, G. J., D. T. Bolvin, E. J. Nelkin, D. B. Wolff, R. F. Adler, G. Gu, Y. Hong, K. P. Bowman, and E. F. Stocker (2007), The TRMM Multisatellite Precipitation Analysis (TMPA): Quasi-global, multiyear, combined-sensor precipitation estimates at fine scales, *J. Hydrometeorol.*, *8*, 38–55, doi:10.1175/JHM560.1.

Kinter, J. L., and c. authors (2013), Revolutionizing climate modeling with project Athena: A multi-institutional, international collaboration, *Bull. Am. Meteorol. Soc.*, *94*, 231–245, doi:10.1175/BAMS-D-11-00043.1.

Martin, E. R., C. Thorncroft, and B. B. B. Booth (2014), The multidecadal Atlantic SST-Sahel rainfall teleconnection in CMIP5 simulations, *J. Clim.*, *27*, 784–806, doi:10.1175/JCLI-D-13-00242.1.

Mathon, V., H. Laurent, and T. Lebel (2002), Mesoscale convective system rainfall in the Sahel, *J. Appl. Meteorol.*, *41*, 1081–1092, doi:10.1175/1520-0450(2002)041<1081:MCSRIT>2.0.CO;2.

Mitchell, T. (2013), Sahel precipitation index, Joint Institute for the Study of the Atmosphere and Ocean, Univ. of Washington, doi:10.6069/H5MW2F2Q.

Mizielinski, M. S., et al. (2014), High resolution global climate modelling; the UPSCALE project, a large simulation campaign, *Geosci. Model Devel.*, *7*, 1629–1640, doi:10.5194/gmd-7-1629-2014.

Mohino, E., S. Janicot, and J. Bader (2011), Sahel rainfall and decadal to multi-decadal sea surface temperature variability, *Clim. Dyn.*, *37*, 419–440, doi:10.1007/s00382-010-0867-2.

Pu, B., and K. Cook (2012), Role of the West African westerly jet in Sahel rainfall variations, *J. Clim.*, *25*, 2880–2896, doi:10.1175/JCLI-D-11-00394.1.

Roehrig, R., D. Bounilol, F. Guichard, F. Hourdin, and J.-L. Redelsperger (2013), The present and future of the West African monsoon: A process-oriented assessment of CMIP5 simulations along the AMMA transect, *J. Clim.*, *26*, 6471–6505, doi:10.1175/JCLIM-D-00505.1.

Scaife, A. A., et al. (2008), The CLIVAR C20C project: Selected 20th century climate events, *Clim. Dyn.*, *33*, 603–614, doi:10.1007/s00382-008-0451-1.

Schneider, U., A. Becker, P. Finger, A. Meyer-Christoffer, M. Ziese, and B. Rudolf (2014), GPCC's new land surface precipitation climatology based on quality-controlled in situ data and its role in quantifying the global water cycle, *Theor. Appl. Climatol.*, *115*, 15–40, doi:10.1007/s00704-013-0860-x.

Skinner, C. B., and N. S. Diffenbaugh (2013), The contribution of African easterly waves to monsoon precipitation in the CMIP3 ensemble, *J. Geophys. Res.*, *118*, 3590–3609, doi:10.1002/jgrd.50363.

Taniguchi, H., W. Yanase, and M. Satoh (2010), Ensemble simulation of cyclone Nargis by a global cloud-system-resolving model-modulation of cyclogenesis by the Madden-Julian Oscillation, *J. Meteorol. Soc. Jpn*, *88*, 571–591, doi:10.2151/jmsj.2010-317.

Tarnavsky, E., D. Grimes, R. Maidment, E. Black, R. P. Allan, M. Stringer, R. Chadwick, and F. Kayitakire (2014), Extension of the TAMSAT satellite-based rainfall monitoring over Africa and from 1983 to present, *J. Appl. Meteorol. Clim.*, *53*, 2805–2822, doi:10.1175/JAMC-D-14-0016.1.

Taylor, K. E., R. J. Stouffer, and G. A. Meehl (2012), An overview of CMIP5 and the experiment design, *Bull. Am. Meteorol. Soc.*, *93*, 485–498, doi:10.1175/BAMS-D-11-00094.1.

Thorncroft, C. D., N. M. J. Hall, and G. N. Kiladis (2008), Three-dimensional structure and dynamics of African easterly waves. Part III: Genesis, *J. Atmos. Sci.*, *65*, 3596–3607, doi:10.1175/2008JAS2575.1.

Walters, D. N., et al. (2011), The Met Office Unified Model global atmosphere 3.0/3.1 and JULES global land 3.0/3.1 configurations, *Geosci. Model Devel.*, *4*, 919–941, doi:10.5194/gmd-4-919-2011.